Computational Materials Science 271 (2026) 114750

Contents lists available at ScienceDirect

Computational Materials Science

journal homepage: www.elsevier.com/locate/commatsci

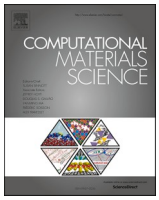

Computational freezing of pentadecane

Sonya Tsibranska-Gyoreva [a,*], Stoyan Iliev [b], Diana Cholakova [a], Anela Ivanova [b,*], Slavka Tcholakova [a], Nikolai Denkov [a]

[a] Department of Chemical and Pharmaceutical Engineering, University of Sofia, 1 James Bourchier blvd., 1164 Sofia, Bulgaria
[b] Department of Physical Chemistry, Faculty of Chemistry and Pharmacy, University of Sofia, 1 James Bourchier blvd., 1164 Sofia, Bulgaria

ARTICLE INFO

Keywords:
Pentadecane
Rotator phase
Molecular dynamics
SAXS
Structural analysis

ABSTRACT

Molecular dynamics simulations are employed to investigate the crystallization of pentadecane-containing systems. Reference crystalline and rotator phase constructed from crystallographic data benchmark the structures formed upon cooling. Phase identification is achieved through global and local structural descriptors, with the fraction of *gauche* conformations and angular P_2 profiles outlined as the most sensitive indicators.

Pentadecane exhibits a markedly more stable rotator phase than hexadecane. This is confirmed by simulations spanning more than 30 K for the reference rotator phase. In this temperature range, a model regular rotator phase of pentadecane remains stable without undergoing significant structural changes, showing high reproducibility across independent trajectories. This contrasts hexadecane, for which a rotator phase rapidly transforms toward a triclinic structure [Iliev et al. 2023]. The presence of a surfactant in the system promotes heterogeneous nucleation, shifts crystallization to higher temperatures, and stabilizes the rotator phase, in agreement with experiments.

A computationally efficient protocol for simulating SAXS spectra from MD trajectories is proposed. The simulated spectra align very well with experimental data for both crystalline and rotator phases. Crystallographic lattice parameters can be extracted from the most intense SAXS peaks, even for experimentally unknown structures, demonstrating the general applicability of the approach to solid-state phase analysis.

1. Introduction

Alkanes and their mixtures form rotator phases—intermediate solid-state arrangements between the isotropic liquid and the fully ordered crystal [1,2]. In the rotator phases, the molecules retain significant rotational freedom, while maintaining long-range positional order in three-dimensional space, similar to that of a crystalline lattice. Rotator phases possess unique rheological properties essential for various technological applications (e.g., cosmetic products, phase change materials, lubricants) and biological functions (e.g., insect wax layers, beeswax shaping, cell membranes), providing plasticity, stability, and adaptive behavior under temperature changes [3].

Rotator phases possess several unusual features, such as surface freezing upon cooling instead of the more common surface melting [4–6]. This phenomenon is influenced by multiple factors, including crystal nucleation, entropy and enthalpy changes associated with molecular immobilization in the crystal lattice, interfacial energy between the crystal and the melt, and thermodynamic parameters of the phase transition in the surface layer [1,7,8]. These characteristics are important not only for practical applications involving alkanes [9] but also for understanding phase transitions in lipid-based systems, such as biological membranes and lipid vesicles [1,10].

Experimental studies have explored the freezing and phase behavior of odd-numbered n-alkanes with intermediate chain lengths (C13 to C21). Spectroscopic analysis showed that phase transitions in odd-numbered alkanes are accompanied by discontinuous changes in the intermolecular vibrational coupling, indicating different molecular arrangements [11]. Other investigations measured properties like thermal conductivity and specific heat, observing discontinuities at the solid-liquid transition [12]. Research on alkane mixtures (pure, binary, ternary) showed that joint rotator phases consistently form when the difference in chain length is $\Delta n \leq 3$ [13]. These mixed phases displayed a sharp temperature dependence in their interlamellar spacing upon cooling, with a thermal expansion coefficient about ten times higher than that of pure alkanes [17].

Although rotator phases are well-characterized experimentally, the

* Corresponding authors.
E-mail addresses: st@lcpe.uni-sofia.bg (S. Tsibranska-Gyoreva), aivanova@chem.uni-sofia.bg (A. Ivanova).

https://doi.org/10.1016/j.commatsci.2026.114750
Received 24 February 2026; Received in revised form 16 April 2026; Accepted 28 April 2026
Available online 22 May 2026

molecular-level mechanisms of their formation and the intermolecular structuring remain unclear due to resolution limits of experimental techniques. Thus, molecular modeling is essential to obtain in-depth understanding of the phenomenon. A review by Mukherjee [14] summarizes the studies that have addressed rotator phase transitions in alkanes, but the microscopic mechanisms remain poorly understood and require further investigation.

The literature contains a few theoretical studies focusing on alkanes with odd-numbered hydrocarbon chains with intermediate length. For example, Li et al. [15] used molecular dynamics (MD) with a united-atom force field to investigate surface freezing in C11, C13, and C15 alkanes at the vacuum-alkane surface. They found that both free surfaces remained crystalline while inner layers melted over specific temperature ranges (325–340 K for C15, 305–320 K for C13, and 288–293 K for C11). In the surface monolayer, molecules aligned nearly perpendicular to the surface and formed regular hexagonal packing, similar to that observed in rotator phases. They also found [19] that the surface freezing temperature range, translational disorder along the surface normal, and transverse disorder depend on the alkane chain length—with longer chains showing wider freezing ranges and more disorder.

Several molecular dynamics simulation studies compared various force fields to model the properties of n-alkanes [16,17]. It was found that TraPPE offered the best compromise between accuracy and computational speed for predicting the properties (critical temperature, pressure and density) [20]. However, models like the refined L-OPLS and OPLS-MP significantly improved predictions for condensed-phase properties such as density, viscosity, and conformational ratios, often outperforming older models [21,23]. While no single force field was perfect across all conditions [22], the studies generally identified CHARMM36, L-OPLS, and Williams 7B as the most reliable for reproducing the properties of liquid alkanes [24]. However, for C15, all atomistic force fields incorrectly predicted a transition from herringbone to monoclinic structure [24].

In a recent study, Burrows et al. [18] combined synchrotron SAXS experiments with MD simulations to resolve the rotator R_I phase of C16. The authors placed a fully extended all-trans hexadecane molecule in a simulation box corresponding to experimentally determined crystallographic data. Using the CrystalDiffract software, they generated a SAXS spectrum and demonstrated excellent agreement with the experimental results. This approach enables the generation of CIF files for phases that are not yet available in crystallographic databases, with their validity verified through comparison to experimentally obtained SAXS spectra.

In our previous studies [19,20], we performed atomistic molecular dynamics simulations to study the phase transition of pure bulk hexadecane and hexadecane/surfactant($C_{16}EO_2$)/water systems. Starting from isotropic liquid phase, we simulated cooling at various rates using different force fields to determine reproducibly freezing temperatures and assess the structuring of the solid-state constructs. Our results demonstrated that the developed computational protocol reliably captures the crystallization process and the formation of rotator phases in all systems.

With this robust simulation framework in place, the next logical step is to explore the chemical factors influencing crystallization, specifically the effect of chain parity. Alkanes with even and odd number of carbon atoms exhibit notable differences in symmetry, structure, and physicochemical properties [21]. There are some distinct dissimilarities between the structural and physicochemical properties of the frozen even-numbered and odd-numbered alkanes, due to their different symmetry in *all-trans* conformation, Fig. S1A. Even-numbered alkanes with 14–24 carbon atoms form triclinic crystals; those with 26–38 form monoclinic crystals; and those with 40–66 form orthorhombic structures [22]. In contrast, odd-numbered alkanes with 13–41 carbon atoms crystallize into orthorhombic lattices, while shorter ones adopt triclinic structure [30]. Thermodynamically stable rotator phases are commonly observed in odd alkanes with $\geq$11 carbon atoms [1,23], while such phases appear in much longer even alkanes – with $\geq$22 carbon atoms [31] (Fig. S1B,C). These differences underscore the role of molecular symmetry and packing in crystallization. Another manifestation of this odd-even effect is the observed non-monotonous dependence of several properties [29]. The origin of this odd-even effect can be explained by the different crystal lattices formed by the two sub-classes of alkanes.

The odd-numbered alkanes crystalize in an orthorhombic lattice, which is shared with the R_I and R_V rotator phases. The latter two give rise to the crystallization. Therefore, the energy barrier that should be overcome by the odd-numbered alkanes in the R → C and C → R transitions is relatively small and the related supercooling is ≈1 °C only. In contrast, the even-numbered alkanes ($n < 28$) crystallize in a triclinic lattice of different structure. Therefore, these molecules should rearrange in a different lattice upon R → C and C → R transitions, which is related to a much higher energy barrier and the respective larger supercooling of >3 °C [29].

In order to observe at the molecular level the effect of hydrocarbon parity, we use molecular dynamics simulations to study the crystallization of C15 (n-pentadecane), which is expected to form a stable rotator phase followed by an orthorhombic crystal formation.

In the current study, we investigate the freezing behavior of two alkane-based systems: bulk pentadecane and pentadecane at a planar, surfactant-stabilized interface with water. Thermodynamic analyses are conducted to determine the nature of the phase transitions in each system. The structural order of the frozen phases is evaluated using radial distribution functions (RDFs), the fraction of *gauche* conformations within the crystallites, and the rotational freedom of the molecules about their long axes. The phase state of the resulting crystallites is characterized by three key structural parameters: the tilt angle (θ) of the molecules relative to the crystallite plane, the distortion parameter (D) of the hexagonal lattice, and the azimuthal angle (φ_d). Results for C15 are compared with previous data for hexadecane (C16) [28] to assess the impact of chain parity on crystallization behavior. The corresponding SAXS spectra of the simulated systems are computed and compared with experimental data to validate the simulated models and assess the agreement with the observed phase behavior. The main outcome includes an efficient procedure for simulation of SAXS spectra of ordered systems of quasi-linear molecules, a descriptive picture of the solid phases obtained after freezing of pentadecane (bulk and surfactant-stabilized) and the distinct differences from analogous hexadecane-containing systems. The provided molecular-level description is able to explain some of the experimentally observed features specific for rotator phases of odd-parity alkanes.

2. Materials and methods

The results presented in this study are based on two types of model systems. The first one consists of 440 molecules of bulk pentadecane (approximately 21,000 atoms), referred to hereafter as bulk PEN (Fig. 1A). The second system includes 494 pentadecane molecules and 108 $C_{16}(EO)_2$ surfactant molecules arranged at a planar interface with 2778 water molecules (Fig. 1B). This system contains approximately 41,000 atoms and will be referred to as PEN/Surf/water. (See Table 1.)

Both systems were initially constructed with ordered molecular arrangements: the molecules were placed at the nodes of a regular hexagonal lattice and randomly rotated about their long molecular axes to promote melting. This type of initial arrangement was chosen to enable comparison to the hexadecane systems studied in our previous work [27]. There, detailed procedures for the models construction are given.

Energy minimization was performed on both systems, followed by heating to 350 K at a rate of 1 K/ps in an NVT ensemble. The systems were then equilibrated at that temperature for 200 ns in an NPT ensemble at pressure 1 bar. This procedure yielded fully isotropic liquid phases, which served as the starting configurations for all subsequent molecular dynamics simulations.

The systems were then cooled to 300 K and equilibrated for additional 200 ns under the same NPT conditions. After equilibration at 300

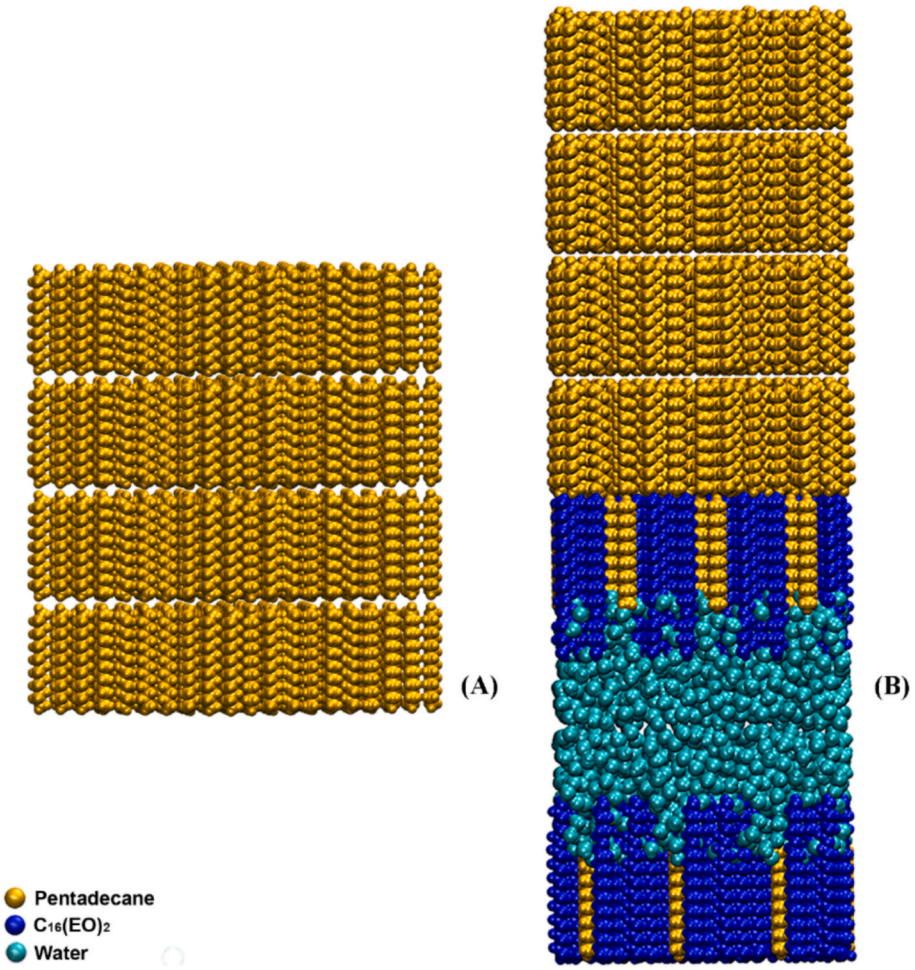

Fig. 1. Illustration of the initial configurations of the studied model systems: (A) bulk PEN and (B) PEN/Surf/water.

Table 1
Calculated structural characteristics of the two reference regular systems. The standard deviation refers to the data averaged over all independent trajectories. The values separated by back slashes correspond to each layer from the herringbone arrangement along the *c* axis.

System	θ, °	D	φ_d, °
Crystal	13 ± 0 / 10 ± 1	0.14 ± 0.00 / 0.15 ± 0.00	6 ± 0 / 6 ± 0
Rotator	11 ± 0 / 9 ± 0	0.13 ± 0.00 / 0.10 ± 0.03	0 ± 0 / 3 ± 4

K, they were further cooled to various lower temperatures to investigate the influence of the final temperature on the formation and type of the ordered phase after freezing. To ensure statistical reliability, each system was simulated in three independent replicas with different initial velocity distributions during the cooling stage. Each cooled system was subsequently simulated for 1000 ns in the NPT ensemble. Additional computational details are provided in the Supporting Information.

Trajectory data were saved every 10 ps. Simulations were performed in a hexagonal periodic box with initial dimensions of 5.2 × 4.5 × 9.0 nm for bulk PEN and 5.2 × 4.5 × 17.2 nm for PEN/Surf/water. The CHARMM36 force field [24] was employed in combination with the TIP4P water model [25,26] both validated in our previous work [26,28] and shown to yield results in agreement with the experimental data.

Additionally, three reference regular systems of bulk PEN were constructed in the orthorhombic symmetry, with and without random molecular rotation about the long axes, to represent the rotator and crystalline phases, respectively. The reference systems are described in detail in the Supporting Information (Fig. S2). It is important to note that three different reference systems were constructed for both the crystalline and rotator phases, corresponding to configurations with a lateral shift along the x direction, a shift along the y direction, and no shift. After MD simulation, all systems converged to an identical structural state, regardless of the initial configuration. The initially imposed shifts (or their absence) were effectively changed, resulting in three equivalent systems corresponding to independent realizations of the same structure, which was then used as reference.

All MD simulations were performed using GROMACS 2020 [27] and visualizations were done with VMD 1.9.4 [28]. Data analyses were carried out using built-in GROMACS tools and custom scripts developed in-house [26].

3. Results and discussion

The results are presented in the following order. Section 3.1 focuses on the characterization of reference solid-state phases of pentadecane. This section includes analyses of *gauche* conformations, rotation about the second principal axis, unit-cell descriptors of the phase state (tilt angle (θ), distortion (D), and azimuthal angle (φ_d)), intermolecular packing assessed through radial distribution functions, and global ordering evaluated from simulated SAXS spectra. The reference regular systems comprise three distinct configurations: one without lateral shifts between layers in the *xy* plane and two with a lateral shift along either the *x* or *y* direction. Section 3.2 addresses the freezing mechanism of pentadecane and presents the same set of structural and orientational parameters evaluated for model systems that crystallized spontaneously upon cooling of isotropic liquid pentadecane.

3.1. Characterization of reference solid state phases of pentadecane

3.1.1. Fraction of gauche conformations

As the molecules transition from a liquid to a crystalline structure, their translational and rotational freedom becomes increasingly restricted and the energetic cost of conformational changes rises. Consequently, a reduction in the number of *gauche* conformations serves as an indicator of increased molecular ordering [29]. For example, the *gauche* fraction has been used as an indicator of phase transitions in C19 [37], and in C16 and C15 [24]. In the present study, we apply the general classification of *trans* and *gauche* conformations to distinguish between the liquid and the solid phases and between the two solid phases per se.

To assess the degree of ordering in the reference regular systems, we analyzed the most reliable structural marker [28] — the percentage of *gauche* conformations in the torsion angles containing methyl groups (Fig. S3).

The average percentages of *gauche* conformations, calculated over the final 100 ns of each of the three independent simulations, see Table S1, are 0.6 ± 0.0% (at 243 K) for the crystalline phase and 8.3 ± 1.7% for the rotator phase (at 310 K), respectively. It is evident that, during the analyzed time period, molecules in the reference crystalline systems remain entirely in the *trans* conformation, whereas the rotator phase exhibits a significantly higher proportion of *gauche* conformations.

The values obtained herein and those reported for hexadecane are in good agreement [28]. In the crystalline structures, the percentage of *gauche* conformations is below 1% for both hexadecane (0.2%) [28] and pentadecane, whereas in the rotator phase it exceeds or is equal to 5% (bulk HEX at cooling rate of 0.1 K/ps). For intermediate states, such as the transition of hexadecane from rotator to crystalline phase, the values of *gauche* conformations fall within an intermediate range between 0.8% and 4.2% [28]. This trend supports the use of *gauche* conformations percentage as a sensitive and reliable indicator for distinguishing between crystalline, rotator, and transitive phases in medium-chain-length alkanes.

3.1.2. Rotation about the second principal axis

Another analysis that well distinguishes the rotator from the crystalline phase is the rotation of the molecules about their long axis [1,2,29]. The second principal axis (P_2) describes the C—C bond orientations of the molecules in the *xy* plane (inset of Fig. 2A). Illustrative data for the angle between P_2 and the *x* axis of the coordinate system are shown in Fig. 2.

It is clearly observed (Fig. 2A) that for the crystalline reference system there is a single narrow prominent central peak at 0°, accompanied by two smaller satellite peaks at ±95°. The area of the satellite peaks accounts for ~15% of the total, indicating that only about 15% of the molecules possess significantly higher rotational freedom. These are likely the molecules at the periphery of the crystallite, which may still exhibit a higher degree of rotational mobility due to differing forces caused by the dissimilarly positioned molecules from neighboring crystallites (see Video S1 in the SI).

In contrast to the crystalline reference system, the histogram corresponding to the rotator phase displays a markedly different profile (Fig. 2B). While three peaks are still present – one centered at 0° and two at ±90°, their magnitude is significantly lower and width – broader. Moreover, a non-zero probability for the values of the angle X-P_2 is observed across nearly the entire angular range, reflecting a substantially increased degree of rotational freedom in the rotator phase.

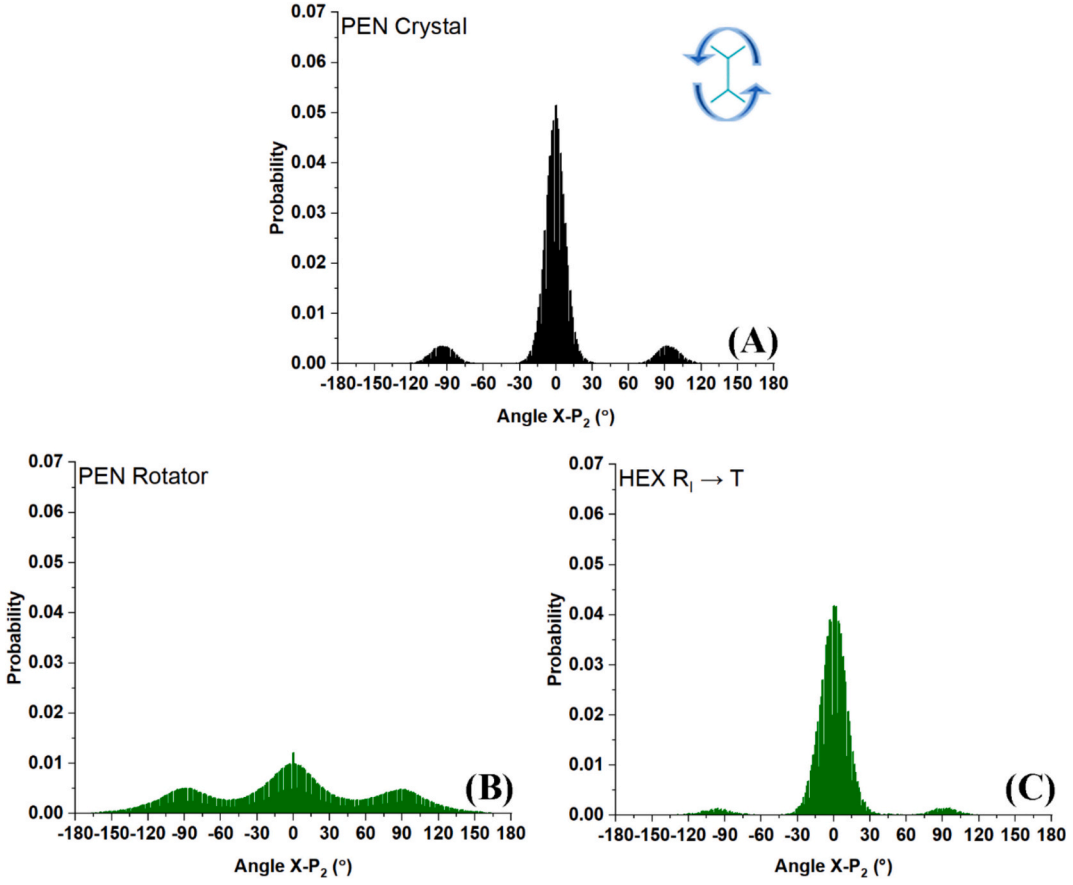

Fig. 2. P_2 orientation profiles of the two reference regular systems: (A) crystal and (B) rotator phase of pentadecane averaged over all independent trajectories and (C) rotator phase of hexadecane; the inset illustrates the direction of rotation along P_2.

The behavior of the pentadecane systems differs from that observed for hexadecane. In the case of pentadecane, both the crystalline and the rotator phases exhibit three peaks in the P_2 histograms: one central and two satellite peaks (see Fig. 2 and Figs. S4 and S5). In contrast, for hexadecane the crystalline phase displays a single, sharp central peak, whereas the rotator phase may exhibit satellite peaks [28]. The difference between the crystalline phases of the two alkanes is expected, given that pentadecane crystallizes in an orthorhombic lattice, while hexadecane adopts a triclinic structure [29,30].

The presence of three peaks in one of the layers of the rotator phase of hexadecane suggests a possible structural similarity to pentadecane. This observation is expected, as the rotator phases of both molecules are known to adopt orthorhombic lattices. The very week population in the satellite peaks in the rotator phase of hexadecane is likely due to a fundamental distinction between even- and odd-numbered medium-chain-length alkanes, namely, the stability of their rotator phases, see Fig. 2C. Pentadecane is expected to form a stable rotator phase, which is supported by the consistent behavior observed across all layers and independent simulations (Fig. S4). In contrast, hexadecane forms a transient and unstable rotator phase, which prevents the clear characterization of a pure rotator state [28,29]. Instead, the system appears to exist in a transition between a rotator phase (orthorhombic, with three peaks in the P_2 histogram) and a crystalline phase (triclinic, with a single central peak in the P_2 histogram). The difference between a stable and an unstable rotator phase is reflected very sensitively in the P_2 profiles, see Fig. 2C.

3.1.3. Unit cell descriptors of the phase state

The next important step of the structural characterization addresses the parameters discriminating the type of the solid state phase. There are three structural parameters that can unequivocally determine the phase state of each system: distortion (D) of the hexagonal packing, which is calculated as 1 – A/B, where A and B are the short and long axes of the ellipse encompassing the six nodes of the hexagonal lattice; azimuthal angle (φ_d) describing the displacement of the first neighbors from the long ellipse axis; tilt angle (θ) of the molecules with respect to the crystallite plane [29]. Each phase is well characterized by these parameters, since each one possesses a distinct combination of the three.

From the analysis of the structural parameters of the reference regular systems (Tables S1, S2 and S3), we observed that alternating molecular layers (i.e., every second layer) exhibited similar parameter values, while differing slightly from the adjacent layers. This pattern was consistently observed in both the crystalline and rotator reference systems, as well as across all independent simulations. Such behavior aligns well with the herringbone arrangement expected for pentadecane [2–6].

The analysis of the three structural parameters reveals moderate tilt of the molecules (not exceeding 13°) in both the crystalline and rotator phases, with slightly smaller (1–2°) tilt in the rotator phase. It is combined with measurable lattice deformation (D ranging from 0.10 to 0.15), again somewhat smaller in the rotator phase. The two layers of the herringbone structure preserve minor differences. Interestingly, in the crystalline phase, the layers with higher tilt have lower D values, whereas in the rotator phase the trend is reversed. This suggests structural differences between the crystalline and rotator phase. The third structural parameter, the azimuthal angle (φ_d), shows more substantial variation between the phases, being ca. 6° in the crystal and negligible in the rotator phase. Among the three structural parameters analyzed, φ_d exhibits the largest contrast between the two phases. Overall, the two reference regular phases are quite similar.

Based on the discussion so far, complemented with some additional statistical assessment (Tables S1, S2 and S3), we conclude that the percentage of *gauche* conformations is the most sensitive descriptor for distinguishing crystalline and rotator phase, followed by φ_d. The distortion parameter (D) and the tilt angle (θ), although structurally meaningful, appear to be less reliable indicators for phase discrimination. The structural analyses indicate that the herringbone structural motif is common for both reference regular systems, which is characteristic of the orthorhombic crystal lattice [1–6,31].

Comparing the molecular tilt angle (θ) for pentadecane and hexadecane reveals that the values for pentadecane are significantly lower, around 10°, whereas for hexadecane they are higher, approximately 15–20°. This is in good agreement with the experimental data, where the lattice parameter *c* for pentadecane corresponds to an almost fully extended *all-trans* conformation [17], while *c* for hexadecane is slightly shorter than the length of the fully extended molecule, suggesting a molecular tilt [32]. The most likely explanation for this difference lies in the distinct crystal lattices of the two alkanes. The triclinic lattice, characteristic of hexadecane, is the most ordered crystal structure and is associated with larger tilt angles of around 20° [1,40]. In contrast, the orthorhombic crystalline and rotator phases of pentadecane feature smaller tilt angles. In our previous study on hexadecane [28], the phases observed were transitive between a rotator phase with an orthorhombic lattice and a crystalline phase with a triclinic lattice, resulting in larger tilt angles compared to those observed for pentadecane.

In terms of the distortion parameter D, the results for both phases of pentadecane fall within an intermediate range (0.10–0.15) compared to the values observed for hexadecane, which vary from approximately 0.05 in some systems to around 0.25 in others. This difference between the two hydrocarbons is most likely due to the distinct symmetry of the resulting phases. In the case of hexadecane, the observed phases include the rotator phases R_{III} and R_V, as well as a triclinic crystal phase—both rotator phases are expected to be transient. In contrast, pentadecane is expected to exhibit a stable R_I rotator phase [29]. It is important to note that the experimentally determined values of D for the R_I phase are around 0.1, which is in good agreement with the values obtained in our simulations.

For the third structural parameter, φ_d, it is noteworthy that the crystalline structures of both alkanes exhibit nearly identical angles of approximately 6°, with very small standard deviations. This coincidence is somewhat surprising given the difference in the crystal lattices of the two hydrocarbons. On the other hand, the rotator phase of pentadecane is characterized by significantly smaller φ_d values, close to 0°, whereas the intermediate (rotator-to-crystalline transition) states of hexadecane display considerably higher values. Interestingly, the experimentally reported value of φ_d for the R_I phase is also 0° [29], suggesting that the rotator phase observed in the pentadecane simulations may correspond to the R_I arrangement.

3.1.4. Intermolecular packing assessed by radial distribution functions

To further investigate the local molecular arrangement, in addition to the structural parameters, we employed another widely used characteristic of local intermolecular ordering — the radial distribution function (RDF) between the centers of mass of the molecules [33] (see the SI for details).

When comparing the two reference systems, a clear difference in the first RDF peak is observed (Fig. 3). In the crystalline phase, the peak is narrower and higher, with a shoulder toward larger distances. In contrast, the corresponding peak in the rotator phase is lower and slightly broader. A difference in the peak position is also evident: the center of the peak in the crystalline phase is located at 0.445 nm, while in the rotator phase it is slightly shifted to longer distances at 0.465 nm. This is expected, as molecules in the crystalline phase are more tightly packed. Differences are also visible in the subsequent peaks. In the crystalline phase, they are well-resolved and distinct, whereas in the rotator phase they appear broadened and merged. This is also consistent with the dynamic behavior of molecules rotating about their long axis, which leads to blurred peak positions and reduced local order.

Upon careful inspection of the RDF profiles for the different layers (Figs. S6, S7), a slight difference in the roughness of the second and the third peak can again be observed between pairs of layers with the same tilt angle, which—as discussed earlier—is related to the herringbone structure. This effect is observed in the rotator phase, whereas in the

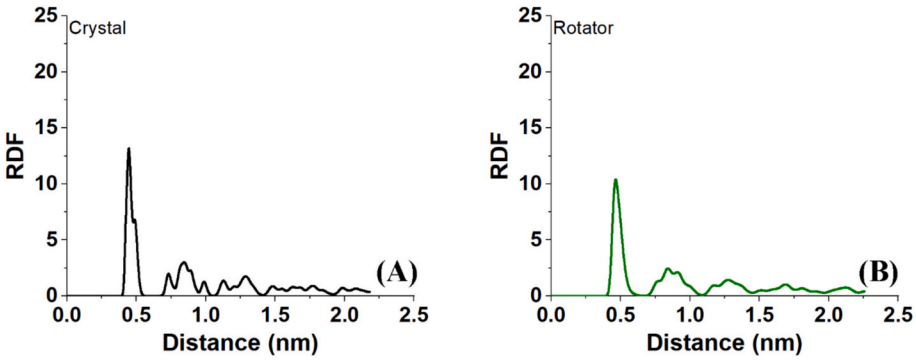

Fig. 3. Representative RDF profiles for the two reference regular systems of pentadecane: (A) crystal and (B) rotator phase averaged over all independent trajectories.

crystalline phase the profiles are nearly identical.

It is interesting to note that the RDF profiles of pentadecane differ significantly from those of hexadecane. While substantial differences between triclinic and orthorhombic crystal lattices are expected, a pronounced distinction is also observed between the rotator phases of the two hydrocarbons, which are both orthorhombic structures (Fig. S8). One might expect that, for the same lattice type, the overall profile would remain similar, which is obeyed for the rotator phase plots of HEX and PEN. However, the shape of the peaks is dissimilar, which may be due to the fact that hexadecane has no stable rotator phase and immediately starts the transition to the crystal. Hence, the peaks for HEX are more split than for PEN.

3.1.5. *Global ordering from simulated SAXS spectra*

As a final step in the characterization of the reference regular systems, we simulated their SAXS spectra. Various methods exist for calculating SAXS profiles from MD simulations, which mainly differ in how solvent contributions are treated [34,35]. The latter is also the main focus of this works. The most frequently applied approaches are developed for biological systems, where explicit solvent effects are essential. It turns out that increasing q-space resolution primarily smoothens the spectra without introducing additional peaks. Importantly, the appearance of multiple peaks is instead related to reflections from different crystallographic planes rather than to numerical resolution. It is suggested that explicit solvent models are preferable for comparison with experimental data, while implicit solvent methods may serve as efficient reaction coordinates for on-the-fly sampling.

In the domain of simulations of alkane-containing systems, Burrows et al. used SAXS spectra but in a somewhat different context [25]. They used experimental crystal lattice parameters to construct a molecular-level illustration of the unit cell of hexadecane in rotator R_I phase. Then, the validity of the generated CIF file was verified by comparison of a SAXS spectrum generated from it with the experimental spectrum of the system. No SAXS was directly simulated from the MD data in this work.

In the current study, we used the built-in SAXS calculation functionality provided by the GROMACS package to obtain SAXS spectra from the MD-generated structural data. This tool calculates SAXS structure factors for the system based on Cromer's method [35]. To enable comparison between the calculated SAXS profiles and experimentally obtained data, we specified the energy of the incident X-rays as 8 keV during the SAXS calculations, matching the conditions used in the experimental measurements [17].

We believe that the low resolution of the peaks is one of the main challenges in calculating SAXS spectra with MD simulations because of the small size of the models. To verify this, we calculated the SAXS spectrum of one of our reference crystalline systems and obtained a profile with very broad peaks and low resolution (Fig. 4A). This is due to the small size of the system, which contains only 576 molecules arranged in a 12 × 12 × 4 lattice. As a result, a weak signal is expected, both because of the limited number of molecules and the small number of molecular planes, which restricts the number of possible Bravais lattice reflections.

A larger system would yield more detailed and accurate calculated SAXS profiles, but simulating larger systems requires significantly more computational resources. Striking a balance between these two factors is

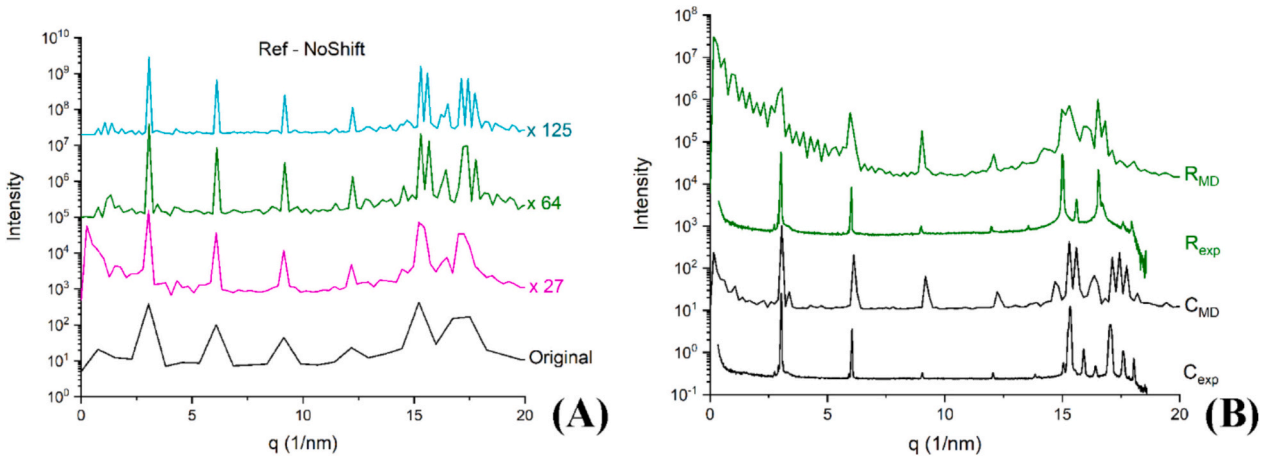

Fig. 4. Representative SAXS profiles: (A) SAXS profiles of the crystalline reference system upon increasing the system size to 27, 64, and 125 times the original simulation box and (B) comparison between the experimental SAXS profile (plots 1 and 3 from the bottom) and the MD-calculated (plots 2 and 4 from the bottom) profiles for both phases: the crystalline phase is denoted in black, whereas the rotator phase is shown in green. (For interpretation of the references to colour in this figure legend, the reader is referred to the web version of this article.)

key when computing SAXS spectra. To address this issue, we enlarged our system by taking the final configuration of our standard system after 1000 ns and replicating it 3, 4, and 5 times along each spatial dimension, resulting in systems which are 27, 64, and 125 times larger, respectively. The advantage of this approach is that we only run MD simulations on the small system—saving computational resources—while using periodic boundary conditions (PBC) to replicate it without creating defects or gaps, thus effectively generating a large single crystal. In this way, we obtain a spectrum corresponding to a much larger system.

As clearly seen from the plots in Fig. 4A, the sensitivity of the analysis has increased drastically upon enlargement of the model. Comparing the obtained results with the experimental data (Fig. 4B) shows a very good agreement in the peak positions. However, we observe some additional peaks in the simulated spectra. This is most likely due to the fact that the replication method produces an ideal single crystal, which is not observed experimentally. We effectively construct an idealized single-crystal structure, which is not representative of real experimental samples that typically exhibit polycrystalline morphology. As a result, additional peaks may appear in the simulated SAXS spectra that are not observed experimentally, due to the absence of finite crystallite size effects and grain boundaries. It is important to emphasize that this step is intended solely to validate the performance of the method.

Based on the obtained SAXS spectra, we determined the orthorhombic lattice parameters a, b, and c for both the reference crystalline and rotator phases. The extracted values for the crystalline phase are: $a = 0.7335$ nm, $b = 0.5112$ nm, $c = 2.0546$ nm, and for the rotator phase: $a = 0.7604$ nm, $b = 0.5175$ nm, $c = 2.0929$ nm. The results are in very good agreement with experimentally reported values [17,38], featuring maximum deviations within 3%, which clearly supports the reliability and accuracy of our reference systems. This validation confirms their applicability as standards for identifying and classifying the spontaneously formed phases in the model systems described in the next sections.

In conclusion, we developed robust analytical tools that allow us to clearly distinguish between the well-ordered reference systems and to analyze spontaneously formed phases.

Next, we proceeded with investigating the crystallization mechanism of pentadecane, specifically the spontaneous formation of ordered structures from molten isotropic state and their analysis using the aforementioned methodologies.

3.2. Freezing mechanism of pentadecane

3.2.1. Phase transition upon cooling

The first step of the analysis of the two types of model systems (Fig. 1) was to identify the type of phase transition occurring therein upon cooling. This can be achieved by interpreting the evolution of the enthalpy profiles during the simulation, as the first-order phase transitions are characterized by a sharp drop in the system enthalpy (in the case of freezing). Furthermore, transitions from liquid to solid are typically accompanied by a change in the density of the respective system. This is observed in all simulated model systems where freezing takes place, indicating that the liquid-to-solid transition is of first order (see examples in Fig. S9). The specific time of this transition may vary between systems.

The quantitative enthalpy change serves as a good initial indicator of the final phase state of the system. It is known that 65–80% of the total phase transition enthalpy can be attributed to the formation of a rotator phase [29].

The enthalpy differences between the liquid and solid phases in our simulated systems, along with their ratios with respect to the experimental transition enthalpy for bulk PEN (from liquid to crystalline phase), are presented in Table S4. For most systems, the enthalpy change exceeds the value typically associated with the transition from liquid to rotator phase, which is 79% for pentadecane [29]. However, none of the systems reached 100%, indicating that a complete transition from the liquid to the crystalline phase did not occur. This suggests that the systems are in an intermediate state between a rotator and a crystalline phase. In the bulk PEN system, two exceptions are observed: 275 K-3 and 278 K-2 (the notation after the temperature refers to the number of the independent trajectory), where the enthalpy change falls below the 79% threshold. For the system containing surfactant, only a single exception is found, 269 K-3. These models are in the early stages of rotator phase.

Interestingly, even when three independent trajectories were run for the same system under identical conditions, the results varied, and the phase state achieved by the end of the simulation differed. This highlights the stochastic nature of crystallization and demonstrates that systems with identical composition can reach different points along the crystallization pathway within the same simulation time at the same conditions.

The obtained results for C15 differ from those observed for hexadecane, where most systems exhibited enthalpy values within the typical range for the liquid-to-rotator phase transition and reached very similar final states [28]. This difference between two hydrocarbons may be related to the fact that the transition between two phases with the same crystal lattice is easier, and additionally, that the rotator phase in pentadecane is stable, i.e. it is energetically favorable for the system to rapidly transition from the liquid to the rotator phase. This is in good agreement with a similar conclusion drawn from experimental data [29].

After confirming the formation and the general type of ordered phases in our systems, the next step was to structurally characterize them. After 1 μs of MD simulation, in the systems where crystallization took place, all investigated trajectories exhibited polycrystalline structures. An illustrative comparison of the two types of models at 278 K is shown in Fig. 5.

A general difference between pentadecane and hexadecane is worth noting. This is the fact that kinks are very common in the crystallites of PEN. This large amount of kinks in PEN is in good agreement with the experimental knowledge that odd-parity alkanes are less densely packed compared to even-parity ones [36].

To structurally analyze the ordered phases in our systems, the individual crystallites are isolated first. The methodology for isolation and the procedure for the analyses done on the isolated crystallites are described in detail in our previous publication [26]. There are some technical aspects (described in the SI) that were changed to improve the efficiency of the methodology. Following the identification of the different crystallites in each system, only the largest crystallite from each system was used for the subsequent detailed structural analyses (Fig. 6), as it is expected to be the most representative and to provide the most statistically reliable information about the phase behavior. To ensure the robustness of this approach, additional analyses were performed on multiple crystallites for selected systems, yielding consistent results and further supporting the validity of our methodology and conclusions.

Snapshots of all investigated crystallites are provided in Fig. S10. As seen, all crystallites are sufficiently large, with the exception of the PEN/Surf/water model 277 K-3. It is important to note that the images in Figs. 6 and S10 do not necessarily represent the entire crystallite but rather only the portion used for the structural analyses (Fig. S11).

3.2.2. Fraction of gauche conformations

The fraction of *gauche* torsion angles in the representative crystallites shows intermediate values (Table 2) in most of the investigated systems below 278 K. This is typical for crystallites in transition between rotator and crystalline phase. Specifically, the *gauche* content remains between 1.1% and 3.8% across temperatures in the range 269–277 K (except for two systems at 269 K).

At 278 K, a significant increase in the percentage of *gauche* conformations is observed in both systems. The value exceeds 5%, which was specified above as the critical threshold for a rotator phase. This suggests that at this temperature the obtained structures of both models are in rotator phase. However, it is again evident that, at the same

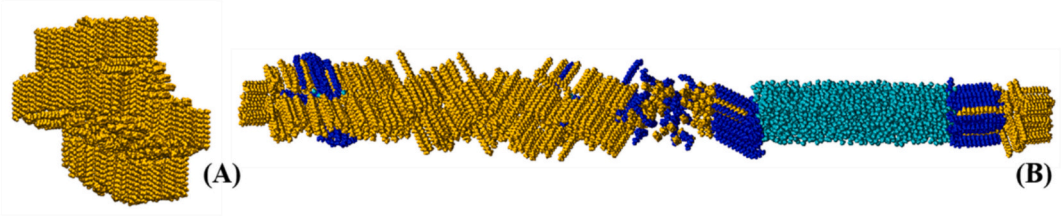

Fig. 5. Illustration of two of the studied model systems: (A) bulk PEN and (B) PEN/Surf/water at 278 K, configuration 1.

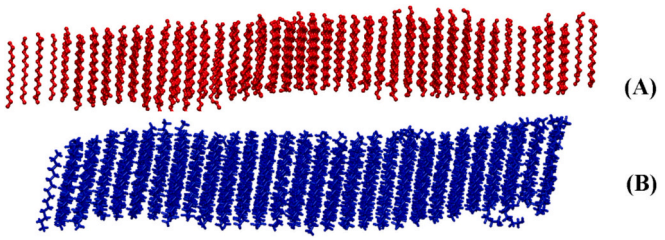

Fig. 6. Illustration of two of the studied crystallites after processing to reconstruct the real-space coordinates of the molecules with the procedure proposed in our previous work [26]; (A) Bulk PEN at 269 K and (B) PEN/Surf/water at 269 K.

Table 2
Percentage of *gauche* conformations in the methyl-containing torsion angles of pentadecane in the two types of model systems. Values from the three independent simulations are given in parentheses.

Temperature	Bulk PEN	PEN/Surf/water
269 K	4.2 ± 0.9 (3.2; 4.7; 4.6)	2.3 ± 0.3 (2.6; 2.1; 2.2)
273 K	3.2 ± 1.0 3.8; 2.1; 3.9)	–
275 K	2.5 ± 1.5 (1.1; 2.2; 4.2)	–
277 K	2.2	1.8 ± 0.6 (2.4; 1.6; 1.2)
278 K	**5.8 ± 3.9** (5.7; 9.7; 1.9)	**5.0 ± 1.6** (6.5; 5.3; 3.3)
282 K	–	3.0 ± 2.0 (1.9; 5.4; 1.7)
350 K (liquid)	40	40

temperature, different independent simulations (Table 2, values in parentheses) yield varying fractions of *gauche* defects, which provides direct confirmation that the systems have reached different points along the crystallization pathway. This is well illustrated by the appearance of well-ordered systems at the higher 278 K and 282 K and of rotator phases at the lower 269 K.

At 350 K, corresponding to the liquid state, the *gauche* content rises significantly to 40%, which clearly distinguishes the disordered state from the ordered phases. These values confirm the high level of conformational order in the crystalline and rotator-like states and support the structural classification of the observed crystallites.

At this point, it is important to clarify the substantial difference between the temperature range observed in our simulations and that reported experimentally. In general, this temperature shift was investigated in our previous work and was attributed to the nano-size of the simulated systems [27]. Therefore, to identify the most appropriate temperature for simulating the reference regular rotator phase, we performed simulations over a broad temperature range from 281 K to 340 K. The phase state was determined based on the percentage of *gauche* defects. The results shown in Fig. S12A reveal a stable rotator phase over a wide temperature interval (300−330*K*), which is in very good agreement with experimental observations regarding the range of stability of this phase [17].

At temperatures below 300 K, the number of *gauche* defects decreases markedly, indicating a transition to a crystalline structure, whereas above 330 K melting occurs and an isotropic liquid phase is formed. It should be emphasized, however, that the absolute temperatures differ significantly from the experimental values. While such deviations during cooling are expected due to supercooling effects associated with the small system size [27], discrepancies of this kind are not generally anticipated for melting transitions.

To examine whether this shift is related to the size and morphology of the ordered structure, we performed an analogous analysis on a spontaneously crystallized system exhibiting a polycrystalline structure composed of multiple crystallites with different orientations. In this case, a similar qualitative behavior was observed but the transition temperatures were shifted toward lower values by approximately 20 K. This effect has also been reported in previous molecular dynamics studies of various systems [37,38], where it was shown that the melting temperature of polycrystalline structures is considerably closer to the experimentally measured value. In addition, experimental studies have demonstrated that melting can initiate at grain boundaries within the solid, occurring several degrees (≈5 K) below the bulk melting temperature, further supporting the observed shift in polycrystalline systems [39]. In addition to the dominant effects discussed above, the observed discrepancy may also be marginally influenced by the force field parametrization, particularly for solid-state properties and first-order phase transitions.

It is observed that in all systems the fraction of *gauche* defects increases with increasing temperature. Up to approximately 18% *gauche* defects, a rotator phase is observed and the structure remains relatively ordered, whereas further increase leads to melting. To verify this behavior, the P_2 profiles of the systems were also analyzed. As an illustration, the P_2 profiles for the PEN/Surf/water at 277 K are presented on Fig. S12B and C. At low temperature, a sharp peak centered at 0° with two very weak satellite peaks is observed (Fig. S12B), indicating a highly ordered structure. After heating and subsequent relaxation for 200 ns at 300 K, the peak broadens significantly, spanning from −90° to +90° (Fig. S12C), which reflects a transition from a more ordered to a less ordered structure, i.e., from a crystalline-like state toward a rotator phase.

It is also evident from the data in Fig. S12A that even at the same temperature the system can populate different structural states: one that is closer to the rotator phase (circles), falling within the green region, and another with a very low percentage of *gauche* defects (squares), indicative of a structure tending toward a crystalline phase. This observation further confirms that, due to the stability of multiple states with very similar energies, the system can exist and remain relatively stable in different structural configurations at the same temperature.

The three temperature ranges identified from this test were used to rationalize the results throughout the manuscript.

3.2.3. Rotation about the second principal axis

Next, we analyzed the rotation of molecules about their long axis (angle *X-P*$_2$) in all representative crystallites. A wide variety of molecular rotation angle distributions were observed for the two systems,

(Fig. 7A, B and Figs. S13, S14).

For bulk pentadecane, several distinct rotational distribution patterns emerged, as shown in Figs. 8A and S10. They varied from a rotational fingerprint with a broad central peak accompanied by a diffuse probability distribution across the full or nearly full angular range, through plots featuring a similar central peak but with two symmetric well-formed shoulders, to a narrow intensive central maximum (Fig. S17) corresponding to strong orientational order and minimal rotational motion. A fourth pattern with a central peak without shoulders (Fig. S13) is the only one resembling the characteristic behavior previously reported for hexadecane-containing systems [28].

For the systems in the presence of surfactant (Figs. 8B and S11), a similar diversity in the molecular rotation profiles was observed. The four patterns are quite alike. The most significant difference is in the satellite peaks – their presence, position or symmetry. For example, while in bulk PEN the satellite peaks are mostly symmetric, many of the PEN/Surf/water systems feature asymmetry. The profile with very weak satellite peaks is reminiscent to that for one of the layers of the rotator phase of hexadecane [28]. The pattern with a single central maximum also resembles previously reported behavior of hexadecane-containing systems [28].

A completely different profile is observed in 277 K-3 of PEN/Surf/water (Fig. S13J). There, a relatively narrow central peak is seen with two pronounced satellite peaks positioned around ±160°, a profile not previously observed in the model crystalline systems or in bulk pentadecane. This behavior indicates that a substantial fraction of molecules undergoes nearly complete rotations within the 100 ns timeframe. This observation suggests that active reorientational transitions are still occurring during the analyzed period. Notably, a similar pattern was detected in one of the surfactant-stabilized systems with hexadecane at a cooling rate of 0.01 K/ps [28]. Hence, this profile may be generally attributed to a system in active rotational transition.

At 278 K and 282 K, more than half of the systems exhibit a broad and diffuse central peak with extended shoulders and non-zero probability across almost the entire angular range, which is a very characteristic fingerprint of a rotator phase. There are some differences in the roughness of the profiles, which may be attributed to random structuring of the system at varying degrees of order between the rotator phase and the crystalline structure (see below).

Interestingly, even at the same temperature, completely different profiles are obtained for pentadecane, depending on the trajectory, which reflects differences in the resulting structures. This clearly demonstrates that, under identical conditions, structurally distinct phases can form. A likely explanation is the intermediate temperature range where the rotator phase in pentadecane is stable but also different packing arrangements, closer to the crystal, may be energetically feasible. Based on the obtained results, it may be assumed that the different microstates are close in energy and, hence, the probabilities of their existence are comparable. Thus, each MD run at similar conditions may end up in a different well on the potential energy surface.

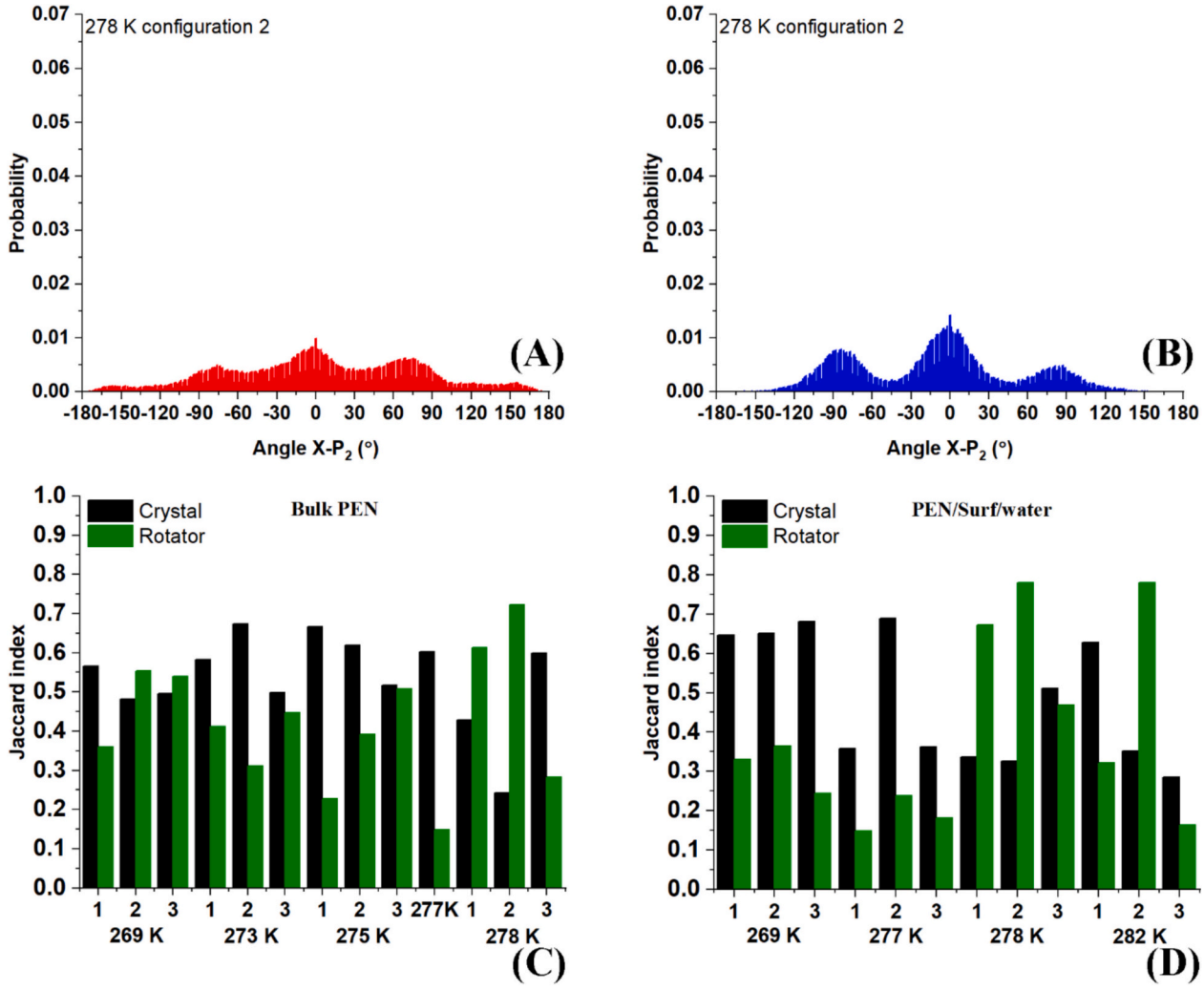

Fig. 7. P_2 orientation profiles of the (A) bulk PEN and (B) PEN/Surf/water systems that have the closest resemblance to the respective profiles of the reference rotator phase; Jaccard indices are given to quantify the resemblance of the model systems with the crystal or rotator phase in: (C) bulk PEN and (D) PEN/Surf/water.

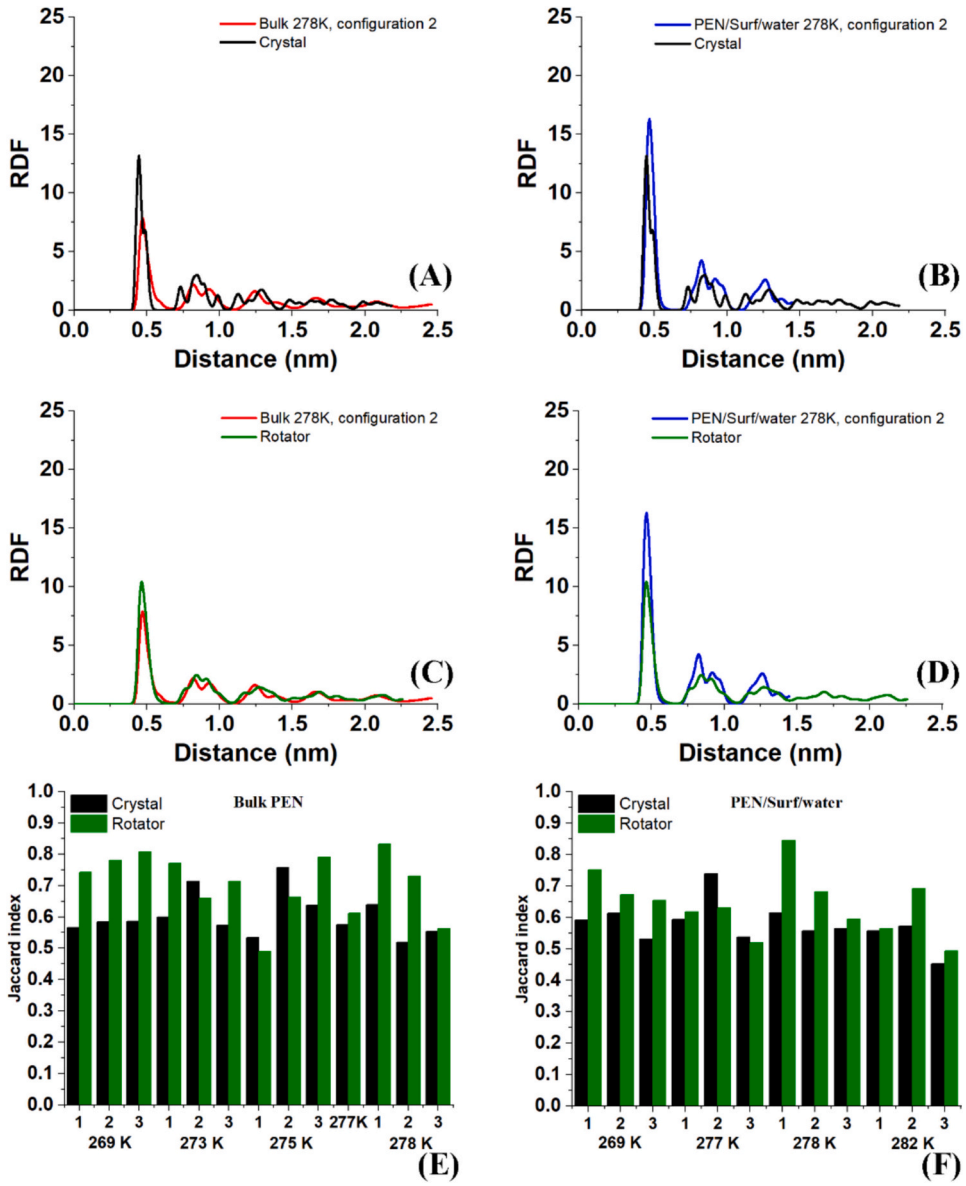

Fig. 8. Intermolecular radial distribution functions of the largest crystallites of (A, C) bulk PEN and (B, D) PEN/Surf/water superimposed on the RDF profiles of the two reference systems; Jaccard indices calculated for (E) bulk PEN and (F) PEN/Surf/water from the RDF profiles of each crystallite compared with the two reference systems.

In this context, some of the observed states are more appropriately described as intermediate or coexistence states rather than strictly defined phases. The shared lattice between crystalline and rotator phases leads to low energy barriers and significant structural overlap, which naturally gives rise to such ambiguity. Nevertheless, analysis of the P_2 angular profiles provides a robust means to differentiate between the various situations. Specifically, it enables identification of crystallites exhibiting predominantly rotator-like behavior (e.g., Fig. S13H), those undergoing a gradual transition toward another structural state with distinct characteristics (e.g., Fig. S14 J), and those corresponding to coexistence regimes where features of both phases are present simultaneously (e.g., Fig. S13 E). In the latter case, the P_2 profiles display signatures consistent with a superposition of the two reference phases behavior.

To quantitatively establish how similar each crystallite is to either of the reference systems, the Jaccard index is calculated [40]. The index quantifies the differences of two plots by their overlapping areas. The index can vary in the range from 0 to 1, where 0 means that the two profiles have no overlap and 1 – that they are identical.

As shown in Fig. 7 C,D, most of the systems exhibit behavior more similar to the reference crystalline phase. However, the values remain $\leq$0.7, indicating a transitive state. Some systems display approximately equal similarity to both reference phases or very low Jaccard indices, suggesting that their structure is distinct from either reference phase. Such behavior is likely to occur during a phase transition. Examples include 269 K-2, 3, 273 K-3, 275 K-3 for bulk pentadecane, and 277 K-1,3, 278 K-3 and 282 K-3 for the surfactant-containing system. In two of the systems, both models at 278 K, configurations 1 and 2, and 282 K-2 for the surfactant-containing system, the profiles show higher similarity with the reference rotator phase—precisely those that also exhibited significantly elevated *gauche* conformations and smeared P_2 profiles.

This analysis further confirms that the structural comparison approach can serve as a reliable method for characterizing the phase state of the systems. The analysis of the Jaccard indices reveals that, overall, at lower temperatures the systems exhibit a greater similarity to the crystalline phase, whereas resemblance to the rotator phase becomes

noticeable for the first time at 278 K. At 278 K and higher temperatures, the rotator phase appears to stabilize, suggesting that it is the most favorable configuration in this range.

The type of rotational motion of the molecules is illustrated further with visualization of the temporal evolution of P_2 (see Videos S1 and S2 in the SI). For the reference systems, it is evident that at 310 K molecules in all configurations undergo nearly continuous rotation, confirming that this is a rotator phase. The molecules rotate freely across the entire angular range, exhibiting essentially no preference for a specific orientation. In the regular crystalline structure, at 243 K, coexistence of two distinct orientations is observed, likely resulting from the herringbone packing. However, in general, the molecules prefer thermal vibrations rather than true rotational motion. In the model systems, four preferred states are observed (see below), populated with varying degree, where clusters of molecules adopt similar orientations. Collective transitions between states occur often, combined with co-existence of two different orientations. This supports the earlier conclusions that most systems are either close to one of the reference phases or are in a transitive state between them and that the molecular transitions occur with minimal energy penalty.

Based on the video analyses, we classified the systems according to their dominant (i.e., most preferred) molecular orientation with respect to their neighbors into four groups. Their specifics are described in the SI (Figs. S13, S14 and S17). Phase analysis suggests that alignments 1 (Video S3) and 2 (Video S4) (with first neighbors displaced in two or one longitudinal dimension) occur with similar frequency in both bulk and surfactant-containing systems, while orientations 3 (Video S5) and 4 (Video S6) (with first neighbors displaced in one perpendicular dimension or not displaced) are observed only occasionally, and more rarely in the presence of surfactant. In contrast, the pure rotator phase is stabilized and its formation is facilitated by the surfactant, appearing in three cases compared to only one in the bulk system, which corresponds well with experimental findings about the surfactants positive impact on rotator phases [17,29].

In general, we may state that surfactant molecules, both at the interface and dispersed as monomers in the bulk, can act as heterogeneous nucleation centers. We hypothesize two main mechanisms by which the surfactant may stabilize the rotator phase. First, the surfactant tends to become more structurally ordered at higher temperatures (around 300 K) than the alkane, thereby promoting crystallization at elevated temperatures where the rotator phase is thermodynamically favored. At these temperatures, the alkane molecules retain sufficient rotational mobility, which facilitates the formation of the rotator phase and effectively extends the temperature range over which it can exist.

Second, the presence of chemically distinct surfactant molecules disrupts the efficient packing of alkane chains into a well-ordered crystalline structure. This hinders the formation of a fully ordered crystal lattice and instead favors the less ordered rotator phase. Taken together, these effects may explain the observed stabilization of the rotator phase in the presence of surfactant molecules.

3.2.4. Unit cell descriptors of the phase state

As a next step, we analyzed the three structural parameters of the representative crystallites: θ, D, and φ_d (Table S5). To ensure a meaningful comparison with the reference regular systems, we used values averaged over the entire reference system rather than per-layer averaging. This approach was chosen because in the crystallites in the model systems, all single-layered, only one of the two molecular orientations from the herringbone structure is present. Therefore, averaging across the whole system provides a more physically meaningful basis for comparison.

It is evident from the data presented in Table S5 that the difference in the θ parameter between the two reference systems is within the standard deviation. Consequently, classification of the model systems based solely on θ is not feasible. Analysis of the D parameter across the model systems shows that only bulk PEN at 277 K exhibits a value within the standard deviation of the crystalline reference. Most of the other systems display a stronger resemblance to the rotator phase, with the exception of bulk PEN 269 K-1 and 275 K-1, 278 K-2, 3 and for PEN/Surf/water 269 K-3, 282 K-1, 2, which cannot be confidently associated with either phase. The φ_d parameter appears to be the most sensitive of the three for distinguishing between the crystalline and rotator phases. Overall, based on φ_d, the bulk PEN systems display a greater resemblance to the crystalline reference structure, indicating that they are further along the transition pathway between the two phases. The reduced sensitivity of θ and D arises from the fact that both crystalline and rotator phases share the same orthorhombic lattice in pentadecane, leading to small structural differences and low discriminative power of these parameters for the specific alkane.

From the above summary, it becomes clear that a definitive classification of the model systems into a specific rotator phase is not possible, in contrast to the hexadecane systems. All examined structures likely exist in intermediate states between the crystalline and rotator phases, and coexistence of both phases within the same system is also plausible, as demonstrated earlier. This complexity arises from the fact that in pentadecane different phases and intermediate states share the same crystal lattice. As a result, they are energetically similar, the energy barriers between them are low, and the phases are both stable and prone to co-existence.

3.2.5. Intermolecular packing assessed by radial distribution functions

The RDF profiles for all analyzed crystallites are shown in Supplementary Figs. S15 to S17. To quantify the structural similarity of each crystallite to the two reference phases, the Jaccard index was calculated [51]. Prior to calculation, the RDFs were truncated at 1.5 nm to eliminate contributions from the noisy long-range tails. The computed Jaccard indices are presented in Fig. 8 E, F.

A direct comparison of the RDFs with those of the reference crystalline and rotator phases is presented for the model systems at 278 K (Fig. 8A–D). For both investigated systems at this temperature, the RDF profiles exhibit significantly higher similarity to the rotator phase reference (Fig. 8C,D), while showing considerable deviation from the crystal (Fig. 8A,B). These results further support the earlier conclusion that the structures formed at 278 K correspond to a rotator phase. The comparable Jaccard indices in this case signify similar packing pattern of the molecules in the studied systems. This is in line with all the findings discussed so far.

3.2.6. Global ordering from simulated SAXS spectra

While the structural parameters and RDF-based comparisons provided valuable insights into the internal organization and phase identity of the crystallites, they offer primarily local or medium-range information. To complement these results and probe the larger-scale structural order in the systems, we further employed SAXS analysis. The SAXS profiles obtained for several of the studied systems are presented in Fig. 9 and discussed below.

Following the SAXS analysis protocol applied to the reference regular systems, the simulation box for the bulk pentadecane system was replicated five times in each direction (see the ×125 SAXS plots in Fig. 9A). As can be seen, the peaks at 278 K are still not sufficiently well resolved. Therefore, we further expanded the system by applying 6 × 6 × 5 and 6 × 6 × 6 replications, corresponding to 180- and 216-fold increases, respectively. The results show that when the expansion is not symmetric (×180), the improvement in resolution is limited, whereas for the symmetric ×216 system the peaks are significantly better separated. These observations suggest that, for bulk homogeneous systems, the most reliable approach is to perform symmetric replication in all directions. Comparison of the obtained spectra with those of the simulated reference crystalline and rotator phases indicates that at both temperatures the system resides in an intermediate state, since the profiles do not match those of the reference phases, while the resulting structures are nonetheless distinct from one another.

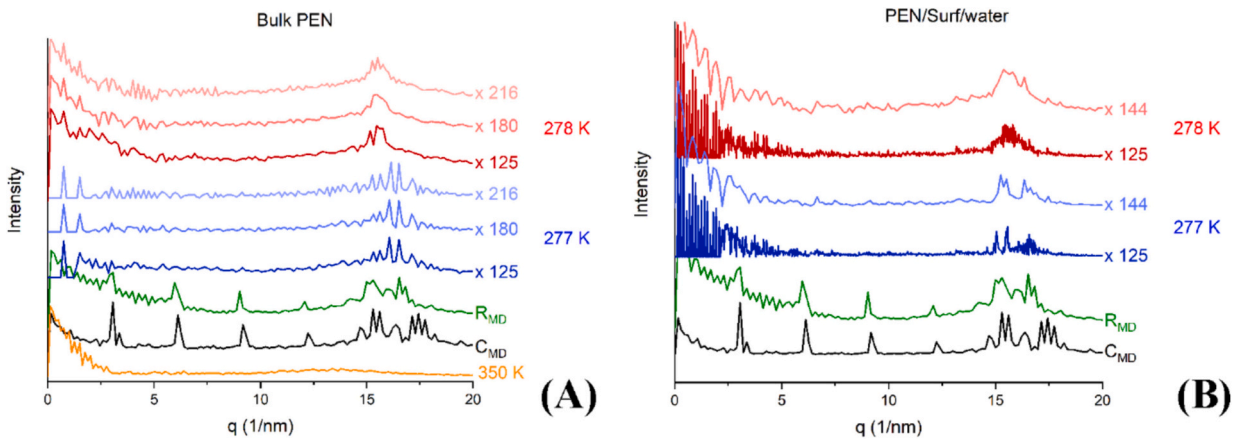

Fig. 9. Representative SAXS profiles for: A) bulk PEN and B) PEN/Surf/water; the crystalline reference system is shown in black, the rotator phase in green, the isotropic liquid in orange, model systems at 277 K-1 in blue, and model systems at 278 K-1 in red. (For interpretation of the references to colour in this figure legend, the reader is referred to the web version of this article.)

Notably, the systems containing surfactant exhibited significantly higher noise levels compared to the bulk models (Fig. 9 B, x125), most likely due to the presence of water. The water layer effectively disrupts the long-range order by preventing further layering and growth of larger crystallites. Moreover, the presence of a large number of water molecules introduces significant noise into the analysis. This results in smaller crystalline domains and consequently increased noise in the scattering signal. To mitigate this issue, particularly in the systems with water, one possible approach is to further replicate the simulation box in the x and y directions and exclude water molecules from the coordinate file used for the SAXS calculation. This would enhance the crystalline signal and reduce noise. To test this approach, we removed the water molecules from the coordinate file and replicated the system $12 \times 12 \times 1$. Replication along the z axis is meaningless because it does not increase the size of the crystallites, as the water layer interrupts the periodicity (in the water-removed system, this appears as a void). Instead, it only increases the total number of molecules and the overall system size, which slows down the SAXS spectrum calculations without providing real improvement. From the x144 plots, it is evident that when water is removed from the coordinate file, the noise level in the signal is significantly reduced. Moreover, replication along the x and y axes by a factor of 12 improved the signal quality, with well-resolved peaks observed at both temperatures.

Symmetric replication improves peak resolution in bulk alkane systems because the structure is polycrystalline, with crystallites exhibiting a wide range of orientations. By replicating the system symmetrically in all directions where periodicity is present, the effective size of the crystallites is increased, leading to a higher number of well-resolved reflections and improved spectral quality.

In contrast, for surfactant-containing systems, asymmetric replication is preferred due to the disrupted periodicity introduced by the interfacial structure. In such cases, replication along directions with preserved periodicity (typically in-plane) provides meaningful improvement, whereas replication along the disrupted direction does not contribute to peak resolution.

In general, replication yields the best results when it is performed in a way that maximizes the effective crystallite size. For bulk homogeneous systems, this is achieved through symmetric replication in all directions, whereas for systems with disrupted periodicity, asymmetric replication along the directions of preserved periodicity is more appropriate.

Comparison with the reference system profiles again reveals that the obtained spectra correspond to intermediate states, which also differ from one another.

We can conclude that the SAXS profiles of the model systems show clear differences compared to those of the reference crystalline and rotator phases (Fig. 9). This supports the hypothesis formulated above that the structures formed in the model systems exist in a transitive state between the rotator and crystalline phases, in agreement with the identified temperature ranges. Additionally, the absence of peaks in the SAXS region (low q) indicates that the obtained crystallites are single-layered.

It is also worth noting that the SAXS profiles of the two model systems at 278 K exhibit a degree of similarity, consistent with all other similarities identified in the previous analyses. This suggests that the two systems at 278 K share a comparable orientation and structural organization and are likely the closest to the ideal rotator phase among all the investigated configurations.

From the SAXS spectra obtained for both systems at 277 K, where a larger number of well-resolved peaks is observed, it is possible to extract the crystallographic parameters of this model system based on the most intense peaks and the crystallographic planes that are expected to give rise to reflections at the corresponding q values. The resulting lattice constants are $a = 0.7602$ nm, $b = 0.5045$ nm, $c = 2.0737$ nm for the bulk PEN system and $a = 0.7560$ nm, $b = 0.5065$ nm, $c = 2.0737$ nm for the PEN/Surf/water system. The c-parameter is adopted from the regular reference systems due to the single-layer nature of the crystallites in the model systems. Alternatively, the length of the fully extended *all-trans* molecule can be used, which eliminates the need for prior knowledge of the reference structure. The obtained values are very close to those determined experimentally [17]: crystalline phase $a = 0.7298 \div 0.7407$ nm, $b = 0.4948 \div 0.4986$ nm, $c = 2.0458 \div 2.0897$ nm, and for the rotator phase: $a = 0.7559 \div 0.7683$ nm, $b = 0.5050 \div 0.5072$ nm, $c = 2.0977 \div 2.1027$ nm. This provides strong evidence that the proposed methodology is capable of extracting crystallographic information even for completely unknown systems, such as those formed spontaneously during cooling, without the need to have experimental data.

In the scenario where experimental data for the investigated phases are available, as in the present case, and a transition between two phases (rotator and crystalline), which exhibit reflections at different q values, is expected, it is possible to verify whether peaks corresponding to both phases are present in the MD SAXS spectra. For all model systems, we observe the simultaneous presence of peaks characteristic of both structures, indicating a transitive state. This behavior is fully consistent with experimental observations, where reflections from the two phases are known to coexist [17]. Notably, only for one system—bulk pentadecane at 277 K—reflections corresponding to the (200) and (111) crystallographic planes of both the rotator and crystalline phases are detected within a single spectrum. This case enables the determination of crystallographic parameters for both structures within the same

system. The extracted lattice parameters for the crystalline phase $a = 0.7331$ nm, $b = 0.5127$ nm, $c = 2.0546$ nm, and for the rotator phase: $a = 0.7609$ nm, $b = 0.5227$ nm, $c = 2.0929$ nm are in very good agreement with experimentally reported values [17]. This demonstrates that the proposed methodology performs very well for both known and previously unknown structures. Moreover, it corroborates all conclusions drawn above, namely, that the systems under investigation exhibit intermediate states in which crystalline and rotator phases coexist.

To summarize, the suggested procedure for SAXS analysis can be carried out on realistic models obtained from MD simulations, including small systems with irregular orientation with respect to the Cartesian coordinate axes. It is recommended that the number of analyzed molecules exceeds 60,000 (in our case, between 60,000 and 100,000) after replication of the periodic box. For bulk systems, replication should be performed symmetrically. In water-containing systems, it is advisable to remove the water from the coordinate file to reduce noise in the analyzed spectra. Furthermore, when water forms a water layer, replication should be performed only along the lateral crystallite directions to effectively improve the spectral quality. Using the developed analysis procedure, SAXS spectra of different systems can be simulated efficiently, and the obtained results show very good agreement with experimental data. Importantly, it is further demonstrated that the methodology remains applicable and provides reliable results even for novel structures. Since the simulated models are relatively small, this approach saves significant computational and experimental time while providing high spectral resolution.

4. Conclusions

The study investigates the crystallization of pentadecane using all-atom molecular dynamics simulations in bulk and at surfactant-stabilized aqueous interfaces, verified against reference systems based on crystallographic data. Phase identification is achieved using structural descriptors, with the fraction of *gauche* conformations and P_2 angular profiles outlined as the most sensitive indicators, while RDFs show more limited discriminative power.

Pentadecane exhibits significantly different behavior compared to hexadecane, forming a much more stable rotator phase over a broad temperature range (>30 K), with facile interconversion between energetically similar states and possible phase coexistence. This is attributed to the structural similarity between its crystalline and rotator lattices. In contrast, hexadecane rapidly transitions to a triclinic phase. The presence of a surfactant promotes heterogeneous nucleation, shifts crystallization to higher temperatures, and enhances rotator-phase stability, in agreement with experimental observations.

A computationally efficient protocol for SAXS simulations is introduced, showing excellent agreement with experimental data. The method captures intermediate ordering and enables extraction of crystallographic lattice parameters even for previously unknown structures, as well as identification of phase coexistence. Overall, the proposed approach provides a robust and generally applicable framework for analyzing solid-state phase behavior in alkane systems.

Supplementary data to this article can be found online at https://doi.org/10.1016/j.commatsci.2026.114750.

CRediT authorship contribution statement

Sonya Tsibranska-Gyoreva: Writing – review & editing, Writing – original draft, Visualization, Resources, Methodology, Investigation, Formal analysis, Data curation, Conceptualization. **Stoyan Iliev:** Writing – review & editing, Visualization, Validation, Software, Methodology, Investigation, Formal analysis. **Diana Cholakova:** Writing – review & editing, Validation. **Anela Ivanova:** Writing – review & editing, Validation, Supervision, Resources, Project administration, Methodology, Conceptualization. **Slavka Tcholakova:** Writing – review & editing, Validation, Supervision, Funding acquisition, Conceptualization. **Nikolai Denkov:** Writing – review & editing, Project administration, Funding acquisition, Conceptualization.

Declaration of competing interest

The authors declare the following financial interests/personal relationships which may be considered as potential competing interests: "Given her role as Editor, Dr. Diana Cholakova had no involvement in the peer review of this article and had no access to information regarding its peer review. Full responsibility for the editorial process for this article was delegated to another journal editor." If there are other authors, they declare that they have no known competing financial interests or personal relationships that could have appeared to influence the work reported in this paper.

Acknowledgements

This study was funded by the Bulgarian Ministry of Education and Science, under the National Research Program "VIHREN", project RotaActive (No. KP-06-DV-4/16.12.2019). The work was supported by a grant from the Swiss National Supercomputing Centre (CSCS) under project ID ch13 for the computational time. S. Tch. acknowledges the support received from European Union-NextGenerationEU, through the National Recovery and Resilience Plan of the Republic of Bulgaria, project No BG-RRP-2.004-0008.

The authors gratefully acknowledge Dr. Eric B. Sirota for the helpful advice and direction provided at key stages of this study.

Appendix A. Supplementary Data

Supplementary material 1: The following data are available as Supporting Information: Additional computational details; Molecular structures and phase diagrams of odd- and even-parity alkanes (Fig. S1); Percentage of *gauche* conformations of the two reference regular systems (Table S1); Illustration of the simulated regular reference systems (Fig. S2); Illustration of the torsion angles used to calculate the *gauche* percentage (Fig. S3); P_2 profiles of all layers in the three crystal regular systems (Fig. S4); P_2 profiles of all layers in the three rotator regular systems (Fig. S5); Calculated structural characteristics of the three crystal regular systems (Table S2); Calculated structural characteristics of the three rotator regular systems (Table S3); RDF profiles of all layers in the three crystal regular systems (Fig. S6); RDF profiles of all layers in the three rotator reference systems (Fig. S7); RDF profiles of reference regular systems of pentadecane and hexadecane (Fig. S8); Illustrative graphs of density profiles of Bulk PEN and PEN/Surf/Water (Fig. S9); Enthalpies of the phase transitions observed during the MD simulations (Table S4); Studied crystallites after processing to reconstruct the real-space coordinates (Fig. S10); Analyzed part of a crystallite with a kink (Fig. S11); Gauche conformation as a function of temperature and P_2 profiles at different temperatures (Fig. S12); P_2 profiles of Bulk PEN (Fig. S13); P_2 profiles of PEN/Surf/water (Fig. S14); Calculated structural characteristics of the model systems (Table S5); RDF profiles of Bulk PEN (Fig. S15); RDF profiles of PEN/Surf/water (Fig. S16); P_2 and RDF profiles of Bulk PEN at 277 K (Fig. S17). Supplementary data to this article can be found online at [https://doi.org/10.1016/j.commatsci.2026.114750].

Data availability

Data will be made available on request.

References

[1] D.M. Small, The Physical Chemistry of Lipids, Plenum, New York, 1986.
[2] E.B. Sirota, Langmuir 13 (1997) 3849–3855, https://doi.org/10.1021/la9704043.

[3] D. Cholakova, K. Tsvetkova, S. Tcholakova, N. Denkov, Colloids Surf. A Physicochem. Eng. Aspects 634 (2022) 127926, https://doi.org/10.1016/j.colsurfa.2021.127926.
[4] B. Ocko, A. Braslau, P. Pershan, J. Als-Nielson, M. Deutsch, Phys. Rev. Lett. 57 (1986) 94–97, https://doi.org/10.1103/PhysRevLett.57.94.
[5] J. Earnshaw, C. Hughes, Phys. Rev. A 46 (1992) 4494–4496, https://doi.org/10.1103/PhysRevA.46.R4494.
[6] X. Wu, E. Sirota, S. Sinha, B. Ocko, M. Deutsch, Phys. Rev. Lett. 70 (1993) 958–961, https://doi.org/10.1103/PhysRevLett.70.958.
[7] P.G. Vekilov, J.J. Yoreo, Rev. Mineral. Geochem. 54 (2003) 57–93, https://doi.org/10.2113/0540057.
[8] J. Dirksen, T. Ring, Chem. Eng. Sci. 46 (1991) 2389–2427, https://doi.org/10.1016/0009-2509(91)80035-W.
[9] A. Sharma, V. Tyagi, C. Chen, D. Buddhi, Renew. Sustain. Energy Rev. 13 (2009) 318–345, https://doi.org/10.1016/j.rser.2007.10.005.
[10] E. Evans, R. Skalak, Mechanics and Thermodynamics of Biomembranes, CRC Press, Boca Raton, FL, 1980.
[11] M. Yamashita, A. Hirao, M. Kato, J. Chem. Phys. 134 (14) (2011) 144503, https://doi.org/10.1063/1.3561879.
[12] C. Velez, J.M. Ortiz de Zarate, M. Khayet, Int. J. Therm. Sci. 8 (4) (2015) 1459–1470, https://doi.org/10.1016/j.ijthermalsci.2015.05.014.
[13] D. Cholakova, M. Pantov, S. Tcholakova, N. Denkov, Cryst. Growth Des. 24 (1) (2024) 362–377, https://doi.org/10.1021/acs.cgd.3c01088.
[14] P. Mukherjee, Phys. Rep. 588 (2015) 1–54, https://doi.org/10.1016/j.physrep.2015.05.005.
[15] H.Z. Li, T.A. Yamamoto, J. Phys. Soc. Jpn. 71 (4) (2002) 1083–1090, https://doi.org/10.1143/JPSJ.71.1083.
[16] I. Ul Samad, N.A. Darwish, M. Qasim, M. Al Zarooni, ACS Omega 7 (44) (2022) 40257–40266, https://doi.org/10.1021/acsomega.2c05175.
[17] A. Burrows, I. Korotkin, S. Smoukov, E. Boek, S. Karabasov, J. Phys. Chem. B 125 (2021) 5145–5159, https://doi.org/10.1021/acs.jpcb.0c07587.
[18] A. Burrows, E. Lin, D. Cholakova, S. Richardson, S. Smoukov, J. Phys. Chem. B 127 (2023) 7772–7784, https://doi.org/10.1021/acs.jpcb.3c02027.
[19] S. Iliev, S. Tsibranska, I. Kichev, S. Tcholakova, N. Denkov, A. Ivanova, Molecules 28 (5) (2023) 2327, https://doi.org/10.3390/molecules28052327.
[20] S. Tsibranska, S. Iliev, A. Ivanova, N. Aleksandrov, S. Tcholakova, N. Denkov, Colloids Surf. A Physicochem. Eng. Asp. 697 (2024) 134466, https://doi.org/10.1016/j.colsurfa.2024.134466.
[21] D. Cholakova, N. Denkov, Adv. Colloid Interface Sci. 269 (2019) 7–42, https://doi.org/10.1016/j.cis.2019.04.001.
[22] M. Broadhurst, J. Res. Natl. Bur. Stand., Sect. A 66A (1962) 241–249.
[23] E. Sirota, A. Herhold, Science 283 (5401) (1999) 529–532, https://doi.org/10.1126/science.283.5401.529.
[24] J.B. Klauda, R.M. Venable, J.A. Freites, J.W. O'Connor, D.J. Tobias, C. Mondragon-Ramirez, I. Vorobyov, A.D. MacKerell Jr., R.W. Pastor, J. Phys. Chem. B 114 (2010) 7830–7843, https://doi.org/10.1021/jp101759q.
[25] W.L. Jorgensen, J. Chandrasekhar, J.D. Madura, R.W. Impey, M.L. Klein, J. Chem. Phys. 79 (1983) 926–935, https://doi.org/10.1063/1.445869.
[26] W.L. Jorgensen, J.D. Madura, Mol. Phys. 56 (1985) 1381–1392, https://doi.org/10.1080/00268978500103111.
[27] M.J. Abraham, T. Murtola, R. Schulz, S. Pall, J.C. Smith, B. Hess, E. Lindahl, SoftwareX 1–2 (2015) 19–25, https://doi.org/10.1016/j.softx.2015.06.001.
[28] W. Humphrey, A. Dalke, K. Schulten, J. Mol. Graph. 14 (1996) 33–38, https://doi.org/10.1016/0263-7855(96)00018-5.
[29] A. Marbeuf, R. Brown, J. Chem. Phys. 124 (2006) 054901, https://doi.org/10.1063/1.2148909.
[30] S. Craig, G. Hastie, K. Roberts, J. Sherwood, J. Mater. Chem. 4 (1994) 977–981, https://doi.org/10.1039/JM9940400977.
[31] N. Wentzel, S. Milner, J. Chem. Phys. 132 (2010) 044901, https://doi.org/10.1063/1.3276458.
[32] D. Cholakova, D. Glushkova, Z. Valkova, S. Tsibranska-Gyoreva, K. Tsvetkova, S. Tcholakova, N.N. Denkov, J. Colloid Interface Sci. 604 (2021) 260–271, https://doi.org/10.1016/j.jcis.2021.06.122.
[33] M.P. Allen, D.J. Tildesley, Computer Simulation of Liquids, Clarendon Press, Oxford, 1987.
[34] M. Bernetti, K. Hall, G. Bussi, Nucleic Acids Res. 49 (2021) e84, https://doi.org/10.1093/nar/gkab459.
[35] P. Chen, J. Hub, Biophys. J. 108 (2015) 2573–2584, https://doi.org/10.1016/j.bpj.2015.03.062.
[36] R. Boese, H. Weiss, D. Blaser, Angew. Chem. Int. Ed. Engl. 38 (1999) 988–992, https://doi.org/10.1002/(SICI)1521-3773(19990401)38:7<988::AID-ANIE988>3.0.CO;2-0.
[37] J. Wang, L. Xu, Y. He, T. Cao, X. Fan, J. Shi, Vacuum 230 (2024) 113616, https://doi.org/10.1016/j.vacuum.2024.113616.
[38] A. Belonoshko, T. Lukinov, L. Burakovsky, A. Rosengren, Eur. Phys. J. Spec. Top. 216 (2013) 199–204, https://doi.org/10.1140/epjst/e2013-01743-1.
[39] S.G. Lipson, E. Polturak, Phys. Rev. B 109 (2024) 024109, https://doi.org/10.1103/PhysRevB.109.024109.
[40] P. Jaccard, Bull. Soc. Vaud. Sci. Nat. 44 (1908) 223–270, https://doi.org/10.5169/seals-268384.